SIN-CHN SCIENTIFIC PRESS PTE.LTD.

Molecular & Cellular Biomechanics 2025, 22(2), 1101.
https://doi.org/10.62617/mcb1101

Article

Study the role of vertebral artery tortuosity and hemodynamics in the association with headache and cerebrovascular diseases

Qiming Zhou[1,†], Chen Feng[2,†], Yibin Lu[1], Dechuan Zhang[2,*], Longling Fan[1,*]

[1] Research Center for Mathematics and Interdisciplinary Sciences, Faculty of Science, Kunming University of Science and Technology, Kunming 650500, China
[2] Department of Radiology, Chongqing Hospital of Traditional Chinese Medicine, Chongqing 400021, China
*** Corresponding authors:** Dechuan Zhang, cqggzdc@163.com; Longling Fan, fan_longling2008@126.com
[†] Contributed equally.

CITATION

Zhou Q, Feng C, Lu Y, et al. Study the role of vertebral artery tortuosity and hemodynamics in the association with headache and cerebrovascular diseases. Molecular & Cellular Biomechanics. 2025; 22(2): 1101. https://doi.org/10.62617/mcb1101

ARTICLE INFO

Received: 19 December 2024
Accepted: 8 January 2025
Available online: 24 January 2025

Abstract: The complex and unpredictable path of the vertebral artery is closely related to symptoms such as headaches, dizziness, and cerebrovascular diseases. This study aims to explore the role of vertebral artery tortuosity and hemodynamics in the association with headaches and cerebrovascular lesion by quantitatively analyzing the morphological parameters and hemodynamics of the vertebral artery. A total of 85 patients with headache symptoms and vascular lesions identified through computed tomography (CT) scans were included. A comparative analysis was then conducted to assess how different levels of vascular tortuosity affect these hemodynamic parameters. These findings indicate that vertebral artery tortuosity is more prevalent among the elderly, women, and patients with headache and vascular disease. A multivariate stepwise Logistic regression analysis highlights the ratio of the distal diameter to the tortuosity index of the left vertebral artery (d1) as a significant risk factor for headache symptoms in patients with vascular lesions. Hemodynamic analysis reveals complex flow patterns within the highly tortuous left vertebral artery, including vortices at areas of significant vascular tortuosity. The left vertebral artery with a high degree of distortion presents with high time-averaged wall shear stress (TAWSS), a high oscillatory shear index (OSI) region, and a low relative residence time (RRT). This discovery not only provides essential reference information for the morphological and hemodynamic analysis of the vertebral artery but also offers critical predictive insights for future clinical evaluations and interventions targeting patients with vertebral artery tortuosity, aiding in predicting their risk of experiencing headaches or the onset of cerebrovascular diseases.

Keywords: headache; cerebrovascular disease; vertebral artery; vascular tortuosity; hemodynamics

1. Introduction

Cerebrovascular diseases can present with a wide range of symptoms, with headache sometimes being the only secondary indicator in certain patients [1]. Jatuzis et al. [2] discovered that headache frequently occurs in those with carotid artery dissection, and a case of vertebral artery dissection has also been reported to be accompanied by migraine. Non-traumatic subarachnoid hemorrhage often results from the rupture of saccular aneurysms located near the circle of Willis, typically presenting with a sudden, severe headache [3]. Harriott et al. [4] revealed that headache incidence in ischemic stroke patients ranged from 6% to 44%, with most headaches exhibiting tension-type characteristics. Notably, posterior circulation strokes and female patients tend to have a higher prevalence of headache. Furthermore, research has linked migraine to the onset of cerebrovascular diseases, particularly among female patients

over 45 years of age [5]. Cerebrovascular diseases continue to pose a threat to public health, as evidenced by the "China Cardiovascular Health and Disease Report 2023" [6], which indicates a persistent increase in cardiovascular disease prevalence in China. It is estimated that China currently harbors 13 million stroke patients, with mortality rates in rural and urban areas standing at 175.58/100,000 and 140.02/100,000 respectively, in 2021. Several cerebrovascular conditions, including subarachnoid hemorrhage (SAH), central nervous system vasculitis, arterial dissection, and cerebral venous thrombosis (CVT), can concurrently cause both headache and stroke, with headache often serving as an early warning sign. Consequently, investigating the prevalence of cerebrovascular diseases among headache patients is of paramount importance [7].

The vertebral artery (VA), being the primary conduit for blood supply to the posterior circulation of the brain, is instrumental in controlling approximately 25% of all strokes within the posterior circulation system [8]. Research indicates that the vertebral artery ranks second in terms of plaque accumulation within the cerebral vascular system [9], with the agglomeration of these plaques ultimately leading to atherosclerosis, a condition that can further precipitate vertebral artery stenosis. Atherosclerosis is intricately linked to a myriad of hemodynamic parameters, whose distribution is significantly influenced by the geometric configuration of blood vessels, thereby modulating the onset and progression of atherosclerosis. Furthermore, vertebral artery stenosis is associated with dire prognoses and elevated mortality rates in posterior circulation ischemic strokes [10].

Notably, the vertebral artery contributes to the intracranial Willis circle's blood supply, hence lesions in the vertebral artery frequently manifest as symptoms such as headaches and dizziness, stemming from inadequate cerebral perfusion. Vascular tortuosity, characterized by excessive elongation and twisting of blood vessels, often exhibiting "S", "C", or pronounced angular alterations, is prevalent in the vertebral artery, particularly in the V1 segment [11]. Given its narrower diameter compared to the carotid artery, the vertebral artery is more susceptible to deformation during excessive atlantoaxial joint movements. For instance, dynamic compression of the vertebral artery can lead to vertebral artery rotational occlusion [12]. The vertebral artery's flexibility and variability render it a site prone to various pathological conditions, posing challenges in identification and diagnosis.

Erosion and vertebral artery stenosis have been extensively studied [13]. Recent examinations of patients with cerebrovascular diseases have additionally uncovered pathological alterations in vascular tortuosity, which are intimately linked to acute ischemic stroke [14]. Consequently, the extent of vascular tortuosity emerges as a predictive indicator for the onset of vascular lesions. An augmentation in VA tortuosity subsequently results in heightened vascular curvature, potentially inflicting local mechanical compression injuries upon the brainstem and/or trigeminal nerve, thereby triggering trigeminal vascular activation and enhancing the predisposition to migraines [15]. Hence, the intensity of headaches experienced by patients is associated with the degree of vascular tortuosity. Hemodynamics, the discipline that delves into the interplay between flow, resistance, and pressure within the cardiovascular system, serves as a fundamental metric for assessing cardiovascular function in clinical practice [16]. Secomb et al. [17] integrated hemodynamic research into circuit analog

analysis, revealing that blood vessel flow resistance is largely independent of flow velocity and is solely contingent upon the geometric attributes of the vessels and blood viscosity. This underscores the profound correlation between vascular tortuosity and alterations in hemodynamics. Furthermore, Cebral et al. [18] observed a robust and significant correlation between the average and peak flow rates of the internal carotid artery (ICA) and VA, suggesting that these two systems are likely to exhibit comparable wall shear stress values. This implies a correlation in blood flow conditions between the ICA and VA. Given the relatively limited research on the VA compared to the ICA, further hemodynamic investigations pertaining to the VA are imperative.

The tortuosity of the VA can induce significant hemodynamic alterations, which subsequently may precipitate headaches and cerebrovascular disorders. Consequently, a quantitative examination of the relationship between VA morphology and hemodynamics holds immense potential in forecasting the occurrence of headaches among patients with cerebrovascular lesions. In this paper, by scrutinizing VA morphology, and identified left vertebral artery (LVA) tortuosity as a pivotal risk factor predictive of headache symptoms in cerebrovascular lesion patients. Notably, previous studies have relatively scantly addressed hemodynamic analyses of vertebral arteries. Therefore, the present study employs computational fluid dynamics (CFD) to conduct three dimensional (3D) reconstructions and data analyses of LVA with varying degrees of tortuosity. This approach enables us to evaluate the hemodynamic consequences of tortuosity in LVA and offers predictive insights for future clinical evaluations and therapeutic interventions, particularly in identifying the concurrence of VA lesions and LVA tortuosity in headache patients.

2. Materials and methods

2.1. Data

Collect data from individuals who underwent head and neck computed tomographic angiography (CTA) examinations at the Radiology Department of a traditional Chinese medicine hospital in Chongqing, spanning from June 2022 to March 2023. Eligibility criteria encompass: (1) Individuals aged 18 years or older; (2) absence of overt intracranial hemorrhage; (3) no significant space-occupying lesions, such as head and neck tumors. Exclusion criteria are: (1) Age below 18 years; (2) occluded arterial blood supply to the head and neck; (3) significant space-occupying lesions, such as brain tumors; (4) image quality insufficient for diagnostic purposes; (5) patients with a defined headache disorder, such as encephalitis, meningitis, recent history of traumatic brain injury, and significant vascular stenosis.

This study included 85 participants (46 males and 39 females, ages 22–45: 13 (15%), ages 46–88: 72 (85%)) aged between 22 and 88 years, with a mean age of 57.53 ± 15.56 years. G*Power software (G*Power 3.1.9.7 for Windows) was used to calculate the sample size. In F tests, the effect size f was set to 0.35, the significance level to 0.05, and the statistical testing power to 0.8. When the experiment was divided into three groups, a total of 84 samples were required for the calculation, while 85 samples in our study were found to be suitable. The cohort included 26 patients (ages 22–45: 0, ages 46–88: 26(31%)) with cerebrovascular lesions and headaches, 31

patients (ages 22–45: 11 (13%), ages 46–88: 20 (24%)) with headaches but no cerebrovascular lesions, and 28 patients (ages 22–45: 2(1%), ages 46–88: 26(31%)) without headaches but presenting with cerebrovascular lesions. Cerebrovascular lesions refer specifically to abnormalities in any of the carotid, internal carotid, or vertebral arteries. Headache symptoms were clinical symptoms of patients without distinguishing the type of headache. All patient data were recorded through medical records. Prior to the examination, all participants provided a signed contrast-enhanced consent form, thereby forgoing the requirement for individual informed consent. The General Electric Company (GE) Revolution 256-row 512-slice spiral CT machine was used for the scanning process, and the Ulrich double-barrel high-pressure syringe was utilized for the high-pressure syringe. The patient was positioned supine with the head first, hands down, head fixed, and a lead apron was used to cover the radiation-sensitive area (gonad). The images were captured from the foot to the head. The lower edge of the scan area displayed the aortic arch, while the upper edge showed the cranial roof. The scanning parameters were as follows: kV: 120, mA: smartmA 200–460, speed: 0.35 s/r, pitch: 0.992:1, layer thickness, and layer spacing: 5 mm, with a reconstruction layer thickness and layer spacing of 0.625 mm. The contrast agent had a concentration of 400 mgI/mL, the flow rate was 3.5–4.5 mL/s, the total dose was 150–300 mg/kg of iodine content, and 40 ml of saline was injected at the same flow rate. The enhanced scan employed the intelligent tracking method, with the monitoring level set at the aortic arch level, the trigger threshold set to 200Hu, a physical delay of 8 s, and a diagnostic delay of 2.2 s.

2.2. Morphological measurement methods

Using the advanced medical image processing software 3D-Slicer, we successfully acquired a 3D reconstruction of the patient's vertebral artery from their head and neck CTA scans, employing an automatic threshold method. This process enabled us to precisely extract the geometric information of the patient's vertebral artery. By implementing a curve method, we positioned each point along the curve at strategic locations within the vertebral artery, thereby creating a curve that mirrors the length of the blood vessel. This allowed us to accurately measure the actual length of the vertebral artery. Subsequently, we connected the vessel's starting and ending points and measured its straight-line distance, which served as the reference for the vessel's straight length. Additionally, we determined the diameter at the terminal end of the vertebral artery, as illustrated in **Figure 1**.

Utilizing the established formula for calculating the tortuosity index (TI = [(actual length − straight length)/straight length] × 100), we derived the tortuosity index for each vessel. Specifically, the tortuosity index of the left vertebral artery was recorded as TI1, while that of the right vertebral artery was recorded as TI2. Furthermore, we employed the formula d = (distal diameter/tortuosity index) × 100 to compute the ratio of the distal diameter to the tortuosity index for each artery. The ratio for the left vertebral artery's distal diameter to its tortuosity index was designated as d1, and similarly, the ratio for the right vertebral artery was recorded as d2 [19].

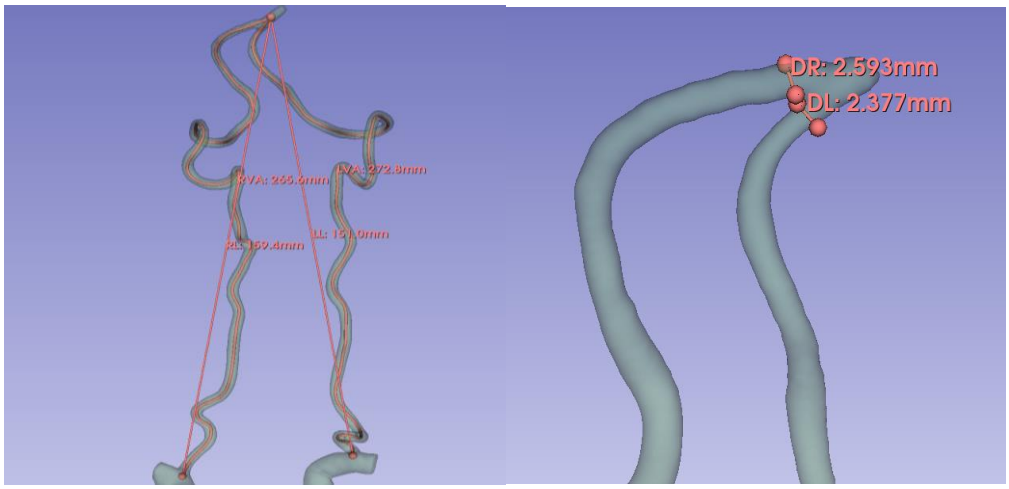

(a) **(b)**

Figure 1. Measuring vertebral artery morphological parameters; **(a)** method for measuring the actual length and straight length of the vertebral artery; **(b)** method for measuring the distal diameter of the vertebral artery. Where RL is the straight length of the right vertebral artery, LL is the straight length of the left vertebral artery, DR is the distal diameter of the right vertebral artery, and DL is the distal diameter of the left vertebral artery [19].

2.3. Computational fluid dynamics simulation

Assuming blood flow is modeled as an incompressible Newtonian fluid, with a specific blood density of $\rho = 1.05 \times 10^3$ kg/m^3 and a viscosity of 3.5×10^{-3} Pa·s, we consider the vessel wall to be rigid and adhering to no-slip conditions. A 3D reconstructed model of the left vertebral artery was generated from head and neck CTA scans, then refined and processed into a computer aided design (CAD) model with smooth boundaries. This refined CAD model then undergoes computational fluid dynamics (CFD) analysis utilizing Ansys software.

The CAD model is imported into Fluent mesh, where hexahedral meshing is employed for partitioning and refinement, resulting in a comprehensive mesh model (MSH format) of the left vertebral artery, The uniform setting of approximately 200,000 grid units for computational fluid models aids in minimizing errors during comparative analysis of calculation results. This ensures that the comparison results and conclusions remain unaffected, and that the quality of the model grid meets the calculation requirements at this scale. Given the study's focus on the interplay between left vertebral artery morphology and hemodynamics, all inlets are uniformly designated as velocity inlets (refer to **Figure 2**) [20], a simplification that does not compromise the results' validity. The outlet is configured as a zero-pressure outlet.

A transient, unsteady-state calculation model is employed, mirroring a typical human heart cycle of 0.8 s, with a time step of 0.01 s. The left vertebral artery MSH mesh model is then introduced into the Parallel Fluent solver for iterative calculations and solutions. Two consecutive cardiac cycles are computed to ensure a stable solution, with data from the second cycle being exported for subsequent in-depth analysis. Finally, the CFD outcomes are visually represented using CFD-Post.

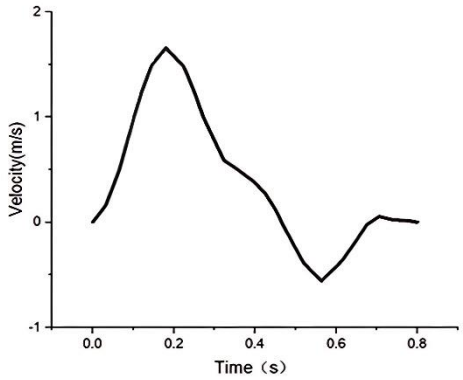

Figure 2. Velocity curve at the entrance of the vertebral artery [20].

2.4. Hemodynamic parameters

Export the spatial coordinates and wall shear stress (WSS) component values of every node at each time point, and compute hemodynamic parameters, including time-averaged WSS (TAWSS), oscillatory shear index (OSI), and relative residence time (RRT), utilizing the formula detailed below [21]. Regions with high OSI offer a more intuitive depiction of the oscillatory shear stress on the vessel wall, which arises from blood flow. The introduction of OSI alone has certain limitations for research, because even blood vessels with excessively curved shapes may have low OSI before the blood vessels are tortuous, resulting in no particularity and may cause large experimental errors. Therefore, we introduce additional high OSI regions as a supplement to better reflect the effect of blood flow changes on the oscillating shear region of the vascular wall. Presently, there is no unanimity in the literature regarding the pathological threshold for high OSI, with values spanning from 0 to 0.5. This article designates 0.4 as the cutoff point, considering nodes exceeding this OSI value (0.4) as high OSI regions, and proceeds to delve into the characteristics of these specific areas.

TAWSS refers to the use of TAWSS to evaluate the average WSS experienced by each vascular wall cell over a cardiac cycle, i.e.:

$$\mathrm{TAWSS} = \frac{1}{T}\int_0^T |\mathrm{WSS}(s,t)|\,\mathrm{dt} \tag{1}$$

where T represents the cardiac cycle, WSS is the instantaneous WSS vector, and s denotes the position on the vessel wall.

In the cardiac cycle, the OSI represents the periodic deviation of the WSS vector from its primary axis, capturing the oscillations in the magnitude and direction of fluid flow by comparing wall shear stresses. Its range is between 0 to 0.5, and the formula for its calculation is:

$$\mathrm{OSI} = 0.5\left[1 - \left(\frac{\left|\int_0^T \mathrm{WSS}(s,t)\mathrm{dt}\right|}{\int_0^T |\mathrm{WSS}(s,t)|\mathrm{dt}}\right)\right] \tag{2}$$

where T represents the cardiac cycle, WSS is the instantaneous WSS vector, and s denotes the position on the vessel wall.

RRT refers to the residence time of particles within the endothelium. Previous studies have shown that RRT serves as a robust measure for low shear and oscillatory shear [22], with its calculation formula being:

$$\mathrm{RRT} = \frac{1}{(1 - 2\mathrm{OSI})\mathrm{TAWSS}} \tag{3}$$

2.5. Statistical analysis

This study used IBM SPSS26.0 (IBM Corp.) software for statistical analysis. The Kolmogorov-Smirnov test was applied for normality testing of measurement data, with normally distributed measurement data presented as mean ± standard deviation, and non-normally distributed measurement data presented as median (1/4–3/4). For normally distributed measurement data, the *t*-test was used for comparative analysis between two groups, while analysis of variance was used for comparative analysis and Chi-square test among three groups. Stepwise binary logistic regression analysis was performed on parameters with diagnostic significance to identify independent influencing factors, with $p < 0.05$ considered statistically significant.

3. Results and discussion

3.1. Analysis of vertebral artery morphological parameters

3.1.1. Analysis of morphological parameters of vertebral arteries in different ages and genders

To analyze the disparities in morphological characteristics of the vertebral artery across various age cohorts, patients were categorized into two distinct groups, utilizing an age threshold of 45 years, as detailed in **Table 1**. The findings revealed that individuals aged 45 and above exhibited an average TI1 value of 49.41 and an average TI2 value of 44.88, in contrast to those under 45 years, who had an average TI1 of 37.80 and an average TI2 of 37.56, with all differences being statistically notable (TI1: $p < 0.001$; TI2: $p = 0.001$). These variations were statistically noteworthy, implying that the prevalence of vertebral artery tortuosity escalates with advancing age.

The comparative analysis of morphological parameters of vertebral arteries across genders is presented in **Table 2**. The outcomes reveal that male patients exhibit an average TI1 of 44.05 and an average TI2 of 40.77, in stark contrast to female patients who possess an average TI1 of 51.87 and an average TI2 of 47.28, with all these disparities demonstrating statistical significance (TI1: $p = 0.002$; TI2: $p = 0.002$). Furthermore, the average d1 for male patients is 6.48, and the average d2 is 5.88, whereas for female patients, the respective averages are 4.81 and 4.72, with all differences being statistically notable (d1: $p < 0.001$; d2: $p < 0.001$). This underscores the fact that male patients exhibit a significantly lesser degree of vertebral artery tortuosity compared to female patients, and that the ratio of distal diameter to tortuosity index of vertebral arteries in male patients is notably higher than that in female patients.

Table 1. Analysis of morphological parameters of vertebral arteries among different age groups.

Indicator	≤ 45 (13)	> 45 (72)	*p*	95%CI
TI1	37.80 ± 1.83	49.41 ± 1.34	< 0.001	−16.28 – −6.95
TI2	37.56 ± 1.50	44.88 ± 1.17	0.001	−11.20 – −3.43
d1	6.52 ± 0.43	5.57 ± 0.22	0.100	−0.18 – 2.10
d2	6.12 ± 0.36	5.21 ± 0.19	0.054	−0.015 – 1.85

Note: $P < 0.05$ indicates statistical significance.

Table 2. Analysis of morphological parameters of vertebral arteries by gender differences.

Indicator	Male (46)	Female (39)	*p*	95%CI
TI1	44.05 ± 1.32	51.87 ± 2.06	0.002	−12.56 – −2.93
TI2	40.77 ± 1.17	47.28 ± 1.69	0.002	−10.50 – −2.53
d1	6.48 ± 0.28	4.81 ± 0.25	< 0.001	0.91 – 2.42
d2	5.88 ± 0.24	4.72 ± 0.20	< 0.001	0.52 – 1.80

Note: $P < 0.05$ indicates statistical significance.

3.1.2. The relationship between headache and cerebrovascular disease with vertebral artery morphological parameters

For patients suffering from cerebrovascular lesions, the occurrence of headache and the morphological attributes of the vertebral artery had been analyzed, as presented in **Table 3**. The findings reveal that the mean TI1 for patients experiencing headache is 52.60, with a mean TI2 of 46.89. In contrast, for patients without headache, the mean TI1 is 47.20, and the mean TI2 is 43.54. This observation hints at a notably higher degree of vertebral artery tortuosity among headache patients compared to those without, albeit the disparity fails to reach statistical significance. Furthermore, the average d1 for headache patients is 4.79, with an average d2 of 4.61. Conversely, for patients without headache, the average d1 is 5.88, and the average d2 is 5.66, with all differences being statistically notable (d1: $p = 0.015$; d2: $p = 0.016$). This suggests that the ratio of the distal diameter to the tortuosity index of the vertebral artery is lower in headache patients than in those without, and this difference is statistically significant.

For individuals suffering from headaches, **Table 4** presents a comprehensive analysis of the occurrence of cerebrovascular lesions along with the morphological parameters of the vertebral artery. The data reveals that patients diagnosed with cerebrovascular lesions exhibit an average TI1 of 52.60, TI2 of 46.89, d1 of 4.79, and d2 of 4.61. In contrast, patients without such lesions have an average TI1 of 43.87, TI2 of 41.33, d1 of 6.34, and d2 of 5.68, with all differences being statistically notable (TI1: $p = 0.007$; TI2: $p = 0.026$; d1: $p = 0.005$; d2: $p = 0.009$). The findings underscore a marked elevation in the degree of vertebral artery tortuosity among patients with cerebrovascular lesions, as compared to those without. Furthermore, the ratio of the distal artery to vertebral artery tortuosity index is notably lower in the latter group, with the observed differences being statistically significant.

Table 3. Analysis of headache in patients with cerebrovascular lesions and the morphological parameters of the vertebral artery.

Indicator	Headache (26)	Without headache (28)	*p*	95%CI
TI1	52.60 ± 2.18	47.20 ± 1.80	0.061	−0.25 – 11.04
TI2	46.89 ± 1.59	43.54 ± 1.95	0.193	−1.75 – 8.44
d1	4.79 ± 0.34	5.88 ± 0.28	0.015	−1.97 – −0.22
d2	4.61 ± 0.29	5.66 ± 0.30	0.016	−1.88 – −0.20

Note: $P < 0.05$ indicates statistical significance.

Table 4. Analysis of cerebrovascular lesions and vertebral artery morphological parameters in patients with headache.

Indicator	Cerebrovascular Lesions (26)	Without cerebrovascular lesions (31)	*p*	95%CI
TI1	52.60 ± 2.18	43.87 ± 2.22	0.007	2.44 – 15.02
TI2	46.89 ± 1.59	41.33 ± 1.79	0.026	0.68 – 10.45
d1	4.79 ± 0.34	6.34 ± 0.39	0.005	−2.61 – −0.50
d2	4.61 ± 0.29	5.68 ± 0.27	0.009	−1.86 – −0.28

Note: $P < 0.05$ indicates statistical significance.

Further detailed examination of the association between headaches and cerebrovascular abnormalities in patients suffering from vertebral artery disease was conducted. Utilizing the occurrence of headaches in patients with vascular lesions as the dependent variable, and statistically significant indicators as independent variables, a multivariate stepwise Logistic regression analysis was undertaken. The findings indicated that d1 ($p = 0.018$, OR = 0.646, 95% CI: 0.449–0.929) represents a significant risk factor for the manifestation of headache symptoms in individuals with vascular lesions. Consequently, the hemodynamic simulation was exclusively focused on the model of the left vertebral artery.

3.2. Hemodynamic analysis of the left vertebral artery

Patients were categorized into three distinct groups, each defined by the tortuosity index (TI1) of the left vertebral artery. Group G1, comprising a low tortuosity cohort of 29 patients (18 males, 11 females), with a TI1 of 36.42 ± 0.71. There are 10 patients in 22–45 age group, and 19 patients in 46–88 age group; Group G2, representing a moderate tortuosity segment of 28 patients (18 males, 10 females), exhibiting a TI1 of 45.32 ± 0.57, There are 3 patients in 22–45 age group, and 25 patients in 46–88 age group; and Group G3, constituting a severe tortuosity set of 28 patients (10 males, 18 females), marked by a TI1 of 61.57 ± 1.32, All patients ranged in 46–88 age group. These categorizations are outlined in **Table 5**. Furthermore, noteworthy variations were observed in age ($p < 0.001$) and age-group ($p = 0.01$) across these diverse tortuosity groups.

Table 5. Relationship between gender, age, and tortuosity index in patients with different degrees of tortuosity.

	G1 (29)	G2 (28)	G3(28)	*p*
Male	18 (62%)	18 (64%)	10 (36%)	0.079
Female	11 (38%)	10 (36%)	18 (64%)	
Age	47.97 ± 2.82	59.21 ± 2.83	65.75 ± 2.05	< 0.001
Age-group				
22–45	10 (35%)	3 (11%)	0 (0%)	0.001
46–88	19 (65%)	25 (89%)	28 (100%)	

Note: $P < 0.05$ indicates statistical significance.

3.2.1. Blood flow velocity

Choose a cardiac cycle featuring a systolic phase (t1 = 0.1 s), a peak systolic moment (t2 = 0.2 s), and a diastolic phase (t3 = 0.3 s). Observe the velocity profiles of severe, moderate, and mild tortuosity depicted in **Figure 3**. The streamline diagram reveals that the flow pattern within the left vertebral artery model experiencing severe tortuosity is intricate, marked by a juxtaposition of high velocities outside the vessel walls and lower velocities within. Consequently, the blood flow velocity at the terminus of this artery is accelerated. In contrast, the left vertebral artery model with mild tortuosity exhibits a more stable flow pattern, characterized by smoother transitions in blood flow velocity, resulting in a reduced velocity at the artery's end. Upon closer inspection of the tortuous segments in all three vessel groups, as highlighted in **Figure 4**, it becomes evident that regions of greater curvature generate eddies, whereas the opposing sides experience heightened flow velocities.

The average flow velocities throughout systole, peak systole, and diastole for the various groups were statistically analyzed and are detailed in **Table 6**. Group G1 exhibited an average flow velocity of 1.26 m/s during systole, 2.09 m/s at peak systole, and 1.08 m/s during diastole. In Group G2, the mean systolic flow velocity was 1.27 m/s, the mean peak systolic flow velocity was 2.10 m/s, and the mean diastolic flow velocity was 1.09 m/s. Group G3 had an average systolic flow velocity of 1.42 m/s, an average peak systolic flow velocity of 2.34 m/s, and an average diastolic flow velocity of 1.22 m/s. Despite the absence of statistical significance between the groups, it was evident that as vessel tortuosity increased, there was a general upward trend in blood flow velocity.

Table 6. The average blood flow velocity of different groups at different times.

period	G1 (29)	G2 (28)	G3(28)	*p*
systole	1.26 ± 0.05	1.27 ± 0.04	1.47 ± 0.09	0.152
Peak systole	2.09 ± 0.08	2.10 ± 0.08	2.34 ± 0.15	0.215
diastole	1.08 ± 0.05	1.09 ± 0.04	1.22 ± 0.08	0.167

Note: $P < 0.05$ indicates statistical significance.

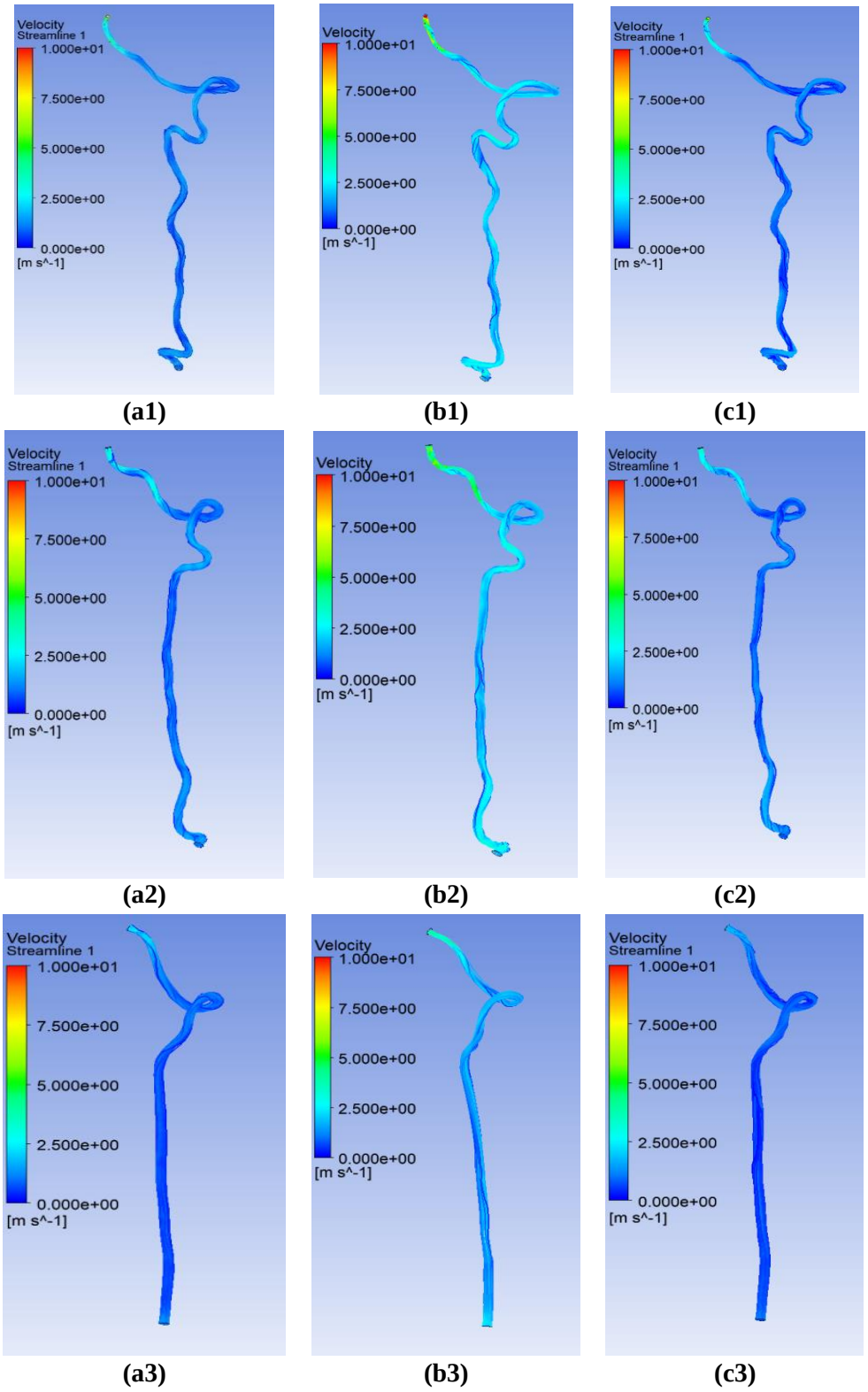

Figure 3. Streamline cloud images of the vertebral artery at different degrees of tortuosity at various times. Where **(a1,b1)** and **(c1)** were the systolic, peak systolic and diastolic blood flow images of patients with severe distortion, respectively. **(a2,b2)** and **(c2)** were the systolic, peak systolic and diastolic blood flow images of patients with moderate distortion, respectively; **(a3,b3)** and **(c3)** were the systolic, peak systolic and diastolic blood flow images of patients with mild distortion, respectively.

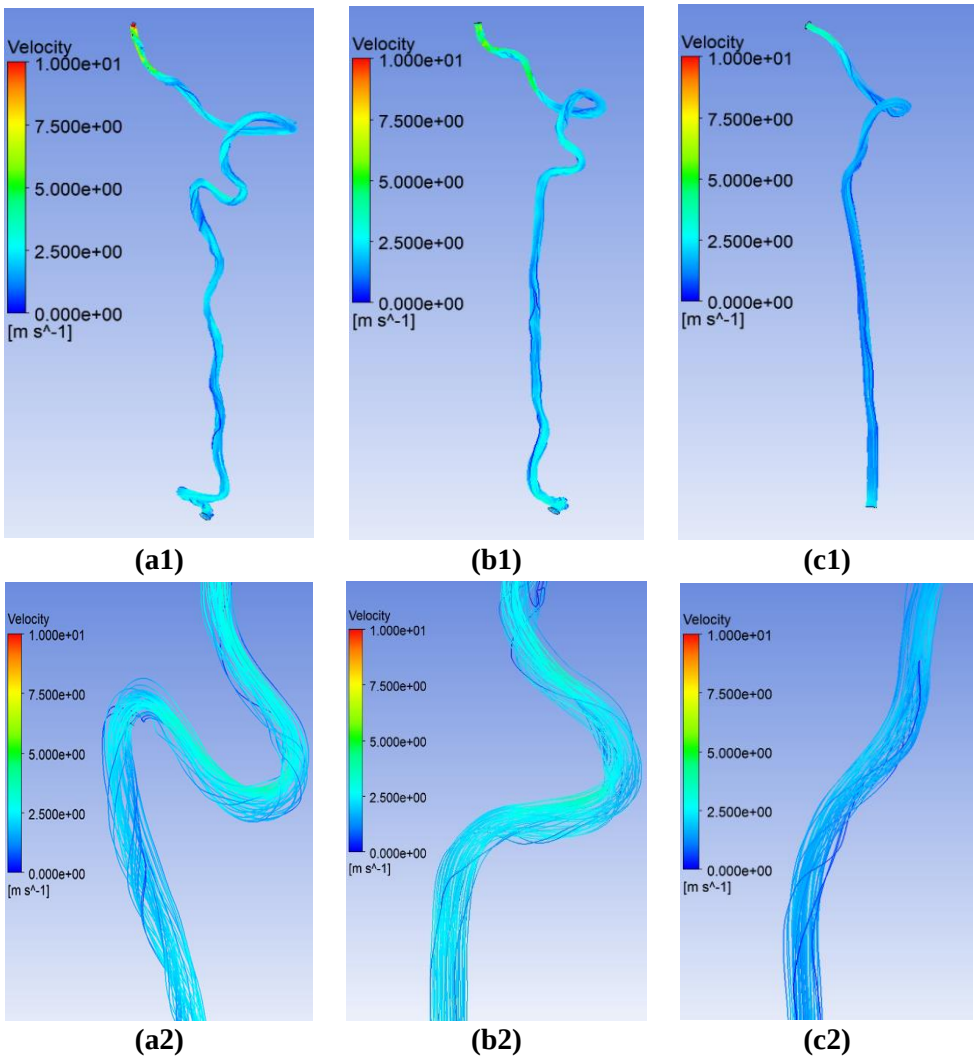

Figure 4. Streamline cloud diagram at the bending site of the left vertebral artery during peak systole in different tortuosity groups. Where **(a1,b1,c1)** are the peak systolic blood flow velocity images of patients with severe, moderate and mild distortion, respectively; **(a2,b2,c2)** are enlarged blood flow velocity images of patients with severe, moderate and mild cardiac systolic vessel tortuosity (black box position in **a1**–**c1** image).

3.2.2. Blood flow velocity

By conducting a deeper analysis of hemodynamic parameters pertaining to WSS, specifically TAWSS, OSI, and RRT, provide insight into the flow dynamics within vessels of varying degrees of tortuosity. To emphasize the influence of tortuosity on these hemodynamic factors, a comparative evaluation was conducted between groups G1, G2 and G3, focusing on TAWSS, OSI, and RRT, as detailed in **Table 7**.

For group G1, the mean TAWSS was recorded as 19.63 pa, accompanied by an average OSI of 0.113 and an average RRT of 0.18 pa^{-1}. Notably, the high OSI region constituted 0.81% of the vessel. For group G2 the mean TAWSS of 20.37 pa, an average OSI of 0.114, and an average RRT of 0.16 pa^{-1}, with a high OSI area of 0.87%. In contrast, group G3 exhibited a higher average TAWSS of 28.80 pa, an average OSI of 0.14, and a lower average RRT of 0.14 pa^{-1}, with a higher high OSI area of 1.01%.

By comparing the three groups, it was found that TWASS and high OSI region increased step by step with the deepening of tortuosity degree, while RRT was on the contrary, with all differences being statistically notable, and the difference was statistically significant, and OSI was not significantly correlated with G1, G2 and G3 groups. These findings suggest that in the context of severely tortuous vertebral arteries, the vessel wall tends to exhibit elevated levels of TAWSS, enlarged high OSI areas, and reduced RRT, underscoring the complex interplay of hemodynamic factors influenced by vessel tortuosity.

Table 7. Comparative analysis of TAWSS, OSI, RRT, and high OSI regions among the three groups.

Indicator	**G1 (29)**	**G2 (28)**	**G3(28)**	***p***
TAWSS(pa)	19.63 ± 1.63	20.37 ± 1.37	28.80 ± 4.23	0.034
OSI	0.113 ± 0.004	0.114 ± 0.001	0.111 ± 0.001	0.689
RRT(pa^{-1})	0.18 ± 0.01	0.16 ± 0.01	0.14 ± 0.01	0.004
High OSI region	0.81 ± 0.05	0.87 ± 0.06	1.01 ± 0.05	0.034

Note: $P < 0.05$ indicates statistical significance.

The cloud maps of TAWSS, OSI, and RRT for various groups of left vertebral arteries are presented in **Figure 5**. Patients exhibiting severe tortuosity exhibit multiple bends in the left vertebral artery, leading to pronounced alterations in blood flow, which results in multiple sections of the vessel wall displaying elevated TAWSS levels. Conversely, patients with mild tortuosity display a smoother vascular path and lesser variability in blood flow patterns, yielding lower TAWSS values on the vessel wall. Patients with moderate to severe tortuosity exhibit a greater number of regions with high OSI, which frequently emerge subsequent to the tortuous segments. In contrast, patients with mild tortuosity demonstrate fewer regions of high OSI. Analogously, patients with moderate to severe tortuosity display a larger number of areas with high RRT, which also appear subsequent to the tortuous segments, whereas patients with severe tortuosity exhibit fewer high RRT areas.

Upon analyzing the spatial distribution of TAWSS and OSI, it becomes evident that both high TAWSS and high OSI areas occur subsequent to vascular tortuosity, and these locations vary significantly (TAWSS: $p = 0.034$; RRT: $p = 0.004$; High OSI region: $p = 0.034$). Specifically, at the site of vascular tortuosity, high TAWSS areas are predominantly located on the inner curvature of the bend, whereas high OSI areas are more prevalent on the outer curvature. Similarly, the occurrence of high OSI and high RRT areas also takes place at positions subsequent to vascular tortuosity.

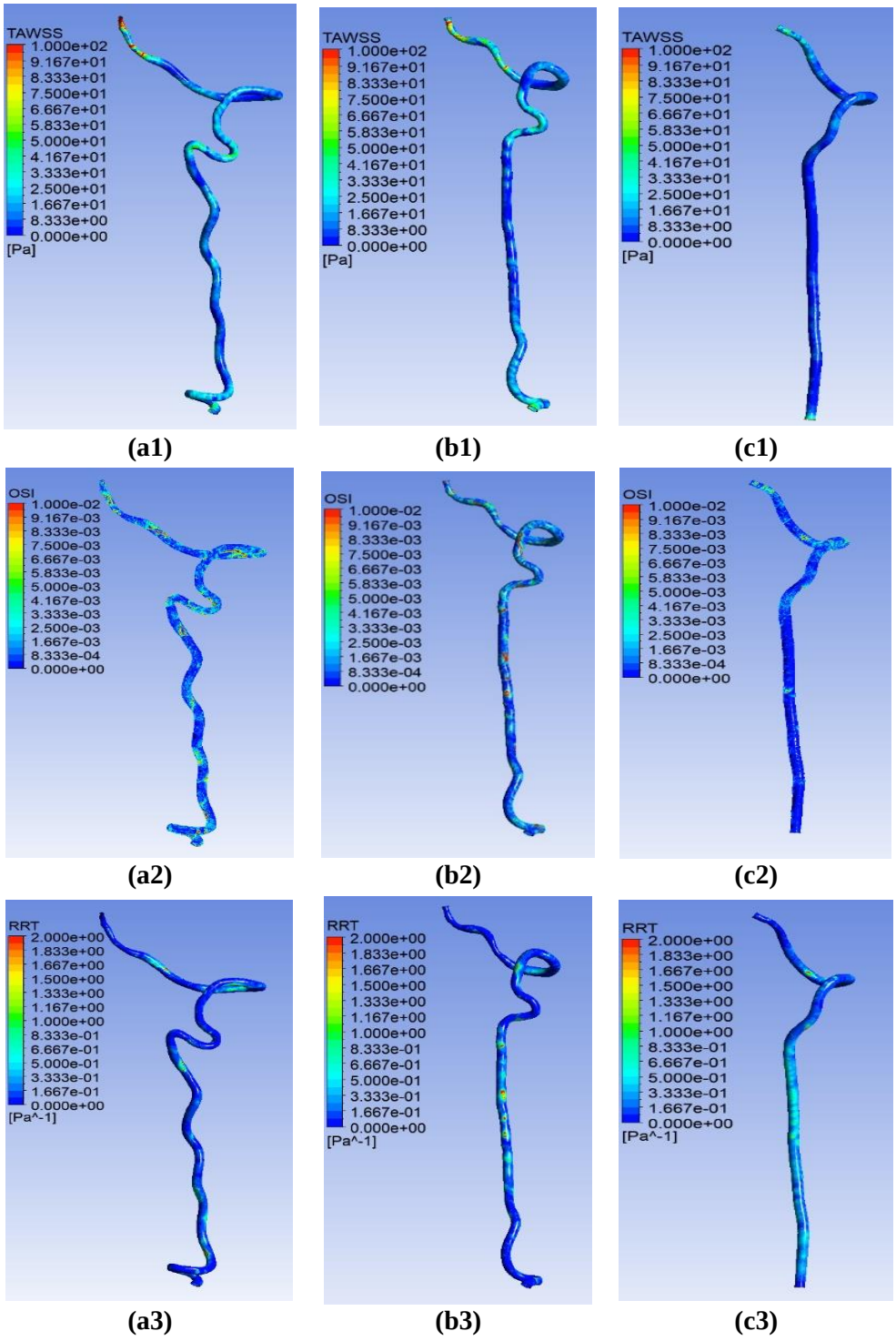

Figure 5. Cloud maps of WSS-related indicators in the left vertebral artery during one cardiac cycle for different groups. Where **(a1,b1)**, and **(c1)** are the distribution cloud maps of TAWSS for patients with severe, moderate, and mild tortuosity, respectively; **(a2,b2)**, and **(c2)** are the distribution cloud maps of OSI for patients with severe, moderate, and mild tortuosity, respectively; **(a3,b3)**, and **(c3)** are the distribution cloud maps of RRT for patients with severe, moderate, and mild tortuosity, respectively.

4. Discussion

This study quantitatively establishes a significant correlation between the left vertebral artery and vascular lesions and headaches in patients. It further delves into the hemodynamic variations among groups exhibiting varying degrees of vertebral artery tortuosity. Notably, the research highlights that individuals aged over 45 and females are predisposed to vertebral artery tortuosity. Among patients with cerebrovascular lesions, a heightened degree of vertebral artery tortuosity and a diminished distal diameter significantly elevate the likelihood of headache occurrence. In patients with headaches, the ratio of distal diameter to tortuosity index in the left vertebral artery is a significant risk factor for headaches linked to vascular lesions. Hemodynamic analysis underscores marked morphological and parameter disparities among vertebral arteries exhibiting different levels of tortuosity. Specifically, severe tortuosity is characterized by a complex flow pattern, featuring elevated TAWSS, high OSI regions, and reduced RRT on the vascular wall, in contrast to the more stable flow observed in mildly tortuous arteries. By enhancing the visualization of flow streamlines at curved segments, the study reveals the presence of vortices in areas of pronounced curvature, accompanied by heightened flow velocities on the opposing side.

As individuals age, the risk of VA tortuosity intensifies. Rothrock et al. [3] segregated cases into two distinct age groups: 0–45 years and 46–90 years. Their findings revealed that patients surpassing 45 years exhibited a notably elevated vertebral artery tortuosity index compared to those within the younger age bracket, aligning with this present research. This observation stems from the fact that aging contributes to a decline in elastin content within vascular walls, subsequently thinning them [23]. When subjected to blood flow pressure, these thinner walls succumb to bending. Furthermore, the aging process prompts degenerative changes in the extracellular matrix and endothelial cells, triggering arterial wall remodeling, stiffening, and twisting. Conversely, with advancing age, the heart accumulates repetitive contractions, potentially leading to ventricular tachycardia, which prompts blood vessels to respond to the unrelenting blood flow pressure, ultimately contributing to vascular tortuosity [24].

Research has discovered that female patients exhibit a higher predisposition to vertebral artery tortuosity in comparison to males. This phenomenon may stem from the inherent geometric stability of the male spine, which, due to its larger stature, offers greater support to the cervical spine. In contrast, the smaller stature of females may contribute to a less stable spine, thereby increasing the vulnerability of their vertebral arteries to tortuosity deformation. Furthermore, the spine's response to dynamic loads is intricately tied to the interaction between the head and spinal components [25], further underscoring the vulnerability of female vertebral arteries. Additionally, hormonal factors play a pivotal role in arterial remodeling, with estrogen promoting a decrease in collagen deposition and an increase in elastin deposition. Conversely, progesterone attenuates the effect of 17-β-estradiol on elastin production, leading to lower levels of 17-β-estradiol in postmenopausal women. This reduction in elastin content subsequently stiffens the blood vessel walls, rendering them more susceptible to tortuosity [26].

Patients suffering from cerebrovascular lesions, who possess more tortuous vertebral arteries and exhibit smaller distal diameters, are more prone to experiencing headaches. Among individuals with headaches, a heightened tortuosity of the vertebral arteries coupled with reduced distal diameters elevates the chances of cerebrovascular lesions. Notably, the ratio of the left vertebral artery's distal diameter to its tortuosity index serves as a pivotal risk factor in determining whether patients with vascular lesions will encounter headaches. Satoshi et al. [27] have revealed that headaches can arise when extension and rotation of the neck trigger vertebral artery dissection, potentially stemming from direct tearing of the vessel wall. The tortuous and variable nature of the vertebral artery makes it prone to various pathological conditions. Excessive twisting may lead to dissection, presenting symptoms such as headaches. Furthermore, Gulli et al. [28] discovered that a diminished vertebral artery diameter escalates the likelihood of posterior circulation stroke recurrence, with vertebral artery stenosis emerging as a significant independent predictor of stroke risk. These findings align with the experimental outcomes presented in this paper, while the analysis delving into the ratio of vessel diameter to its tortuosity index offers further insights into vessel alterations, furnishing an easily discernible indicator for alterations in hemodynamics.

As the level of vascular tortuosity intensifies, notable alterations in blood flow patterns arise, giving rise to intricate flow phenomena like vortices at the sites of tortuosity. Prior research has demonstrated that the recirculation and secondary flows induced by curvature augment the distal outer wall area of the curved artery, which is marked by low and fluctuating WSS [29]. The velocity of blood flow is intricately linked to WSS, with heightened WSS corresponding to increased flow velocity. Nevertheless, regions with low WSS are predisposed to heightened OSI [30]. Vascular tortuosity elicits high-velocity zones on the inner vessel wall, resulting in elevated TAWSS on the inner side and escalated OSI on the outer side at the tortuosity sites. These alterations in blood flow patterns signify that the associated parameters undergo changes, leading to more intricate forces acting on the vessel wall. This enhances the vessel's susceptibility to tortuosity and disease, thereby further exacerbating alterations in blood flow patterns, which may manifest as symptoms such as headaches and dizziness in patients.

Within a cardiac cycle, a heightened OSI value signifies an intensified oscillation of WSS during that period. As the value escalates, the likelihood of inducing endothelial cell dysfunction escalates concurrently, thereby significantly fostering the development of plaques [31]. High OSI regions frequently coincide with vortices, and in comparison to laminar flow, vortices have the capability to stimulate endothelial cells to generate an augmented amount of reactive oxygen species, ultimately contributing to vascular maladies, including arterial deformation and atherosclerosis [21]. Li et al. [29] discerned that the distal outer wall of the curved descending aorta harbors regions of flow recirculation and secondary flow, which evoke oscillations in that vicinity, and they observed heightened OSI regions on the said wall, with the extent of the affected region augmenting in accordance with the augmentation of vascular curvature. This aligns with our research findings. RRT serves as a metric to assess the duration of molecular residence proximal to the lumen boundary, evaluating the surface shear conditions that integrate shear magnitude and

its oscillatory nature [22]. Blood clot formation encompasses diverse mechanisms; venous clots, also known as "red clots", arise from the protracted interplay between platelets, coagulation factors, and endothelial cells at low shear rates, precipitating thrombosis, and these areas typically exhibit elevated RRT [32]. Conversely, arterial clots, associated with alternative etiologies and referred to as "white clots", are linked to high shear rates and platelet aggregation, and they are correlated with atherosclerosis [33]. The outcomes of this study unveiled that in the highly tortuous group, there is a diminished RRT, suggesting the prevalence of high shear rates, which implies that this group is more susceptible to vascular disorders, such as atherosclerosis, a conclusion that resonates with our research.

Overall, for cases exhibiting severe tortuosity, characterized by high TAWSS and OSI areas along with low RRT, there is an elevated vulnerability to vascular diseases, notably vertebral artery stenosis, atherosclerosis, and plaque rupture, which can ultimately precipitate strokes. Consequently, in future endeavors, we will continue to explore the relationship between various types of headaches, cerebrovascular diseases, and cerebral hemodynamics, including the impact of potential factors such as smoking, drinking, and hypertension on human blood flow. Simultaneously, we will conduct long-term follow-up observations to evaluate the long-term effects of vertebral artery malformations on headaches and cerebrovascular lesions. Research on vertebral artery abnormalities remains a focus because they may serve as key indicators of headaches and cerebrovascular lesions. The experimental results presented in this paper offer a theoretical foundation for clinical diagnosis and treatment, particularly for the elderly, women, and patients with vertebral artery distortion as observed by CTA. These results can predict the onset of headaches, dizziness, and cerebrovascular diseases. Additionally, they provide a basis for subsequent studies on the hemodynamics of the left vertebral artery and the conditions of headache and dizziness, thereby further advancing the field of clinical science.

While this study undoubtedly offers profound insights, it is imperative to acknowledge its inherent limitations: (1) The modest sample size may introduce an element of randomness into the findings; (2) considering the spatial resolution limitation and computational efficiency of CTA, this study assumes that the blood vessel wall is rigid. However, under complex blood vessels and high flow velocity conditions, ignoring the influence of the elasticity of the tube wall on the flow velocity may lead to velocity calculation errors. Although this has little impact on the experiment, it does exist.

5. Conclusion

In summary, age and gender significantly influence vertebral artery tortuosity. Patients with vascular lesions and increased vertebral artery tortuosity often have narrower distal diameters and a higher likelihood of experiencing headaches. This correlation also applies to headache patients, where the distal diameter of the left vertebral artery and its associated ratios serve as predictive factors for the development of headaches in those with vascular lesions. Additionally, patients with tortuous left vertebral arteries experience more intricate blood flow velocities, potentially resulting in clinical manifestations like headaches. In cases of severely tortuous vertebral

arteries, the wall of vessel exhibits high TAWSS, areas of elevated OSI, and reduced RRT. Consequently, these findings offer valuable insights for future morphological and hemodynamic analyses of the vertebral artery, while also providing predictive guidance for clinical assessment and treatment of patients with tortuous left vertebral arteries who may suffer from headaches or even develop cerebrovascular diseases.

Author contributions: Conceptualization, QZ and LF; methodology, LF; software, QZ; validation, CF, DZ and LF; formal analysis, QZ; investigation, YL; resources, LF and DZ; data curation, QZ; writing—original draft preparation, QZ; writing—review and editing, LF; visualization, DZ; supervision, YL; project administration, LF; funding acquisition, YL. All authors have read and agreed to the published version of the manuscript.

Funding: Authors also thank the financial support from National Natural Science Foundation of China (No.12461079, 11461037), Yunnan Fundamental Research Projects (No. 202101BE070001-50, 202301AU070184), Chongqing Science and Health Joint Medical Research key Project (No. 2024ZDXM001), and Chongqing Medical Scientific Project (2024WSJK091), and Chongqing Natural Science Foundation project (No. cstc2021jcyj-msxm0727, CSTB2023NSCQ-MSX0295), and Xinglin Scholar Research Premotion Project of Chengdu University of Traditional Chinese Medicine (No. YYZX2022136, YYZX2022130) and Kunming University of Science and Technology Self discipline. Talent Introduction Scientific Research Foundation Project (No. KKZ3202307033).

Ethical approval: The study was conducted in accordance with the Declaration of Helsinki, and approved by Ethics Committee of Chongqing Hospital of Traditional Chinese Medicine (2024-KY-HY-49, 2024.11.19).

Conflict of interest: The authors declare no conflict of interest.

References

1. Diamanti S, Longoni M, Agostoni EC. Leading symptoms in cerebrovascular diseases: what about headache? Neurological Sciences. 2019,40:147-152; https://doi.org/10.1007/s10072-019-03793-8.
2. Jatuzis D, Valaikiene J. Migraine-like presentation of vertebral artery dissection after cervical manipulative therapy. Perspectives in Medicine. 2012,1(1-12):452-454; https://doi.org/10.1016/j.permed.2012.03.010.
3. Rothrock JF, Diener HC. Headache secondary to cerebrovascular disease. Cephalalgia. 2021, 41(4): 479-92; https://doi.org/10.1177/0333102421999045.
4. Harriott AM, Karakaya F, Ayata C. Headache after ischemic stroke: a systematic review and meta-analysis. Neurology. 2020,94(1):e75-e86; https://doi.org/10.1212/WNL.0000000000008591.
5. Wang, M. H., Pan, et al. Prevalence and risk factors of headache in Chinese with stroke: a cross-sectional study based on CHARLS. The journal of headache and pain. 2024, 25(1), 217; https://doi.org/10.1186/s10194-024-01930-z.
6. Liu MB, He XY, Yang XH, et al. Key points of China Cardiovascular Health and Disease Report 2023. Chinese Journal of Cardiovascular Science. 2024,29(4):305-324; https://doi.org/10.3969/j.issn.1007-5410.2024.04.002. (in chinese)
7. Lu J, Liu W, Zhao H. Headache in cerebrovascular diseases. Stroke and Vascular Neurology. 2020,5(2); https://doi.org/10.1177/0333102421999045.
8. Liu C, Zhang C, HOU XX, et al. Morphological difference of vertebral artery on both sides of human body and its effect on hemodynamics. Modern Instrument and Medical Science. 2022,28(05):30-37; https://doi.org/10.11876/mimt202205007. (in chinese)

9. Madonis SM, Jenkins JS. Vertebral artery stenosis. Progress in Cardiovascular Diseases. 2021, 65:55-59; https://doi.org/10.1016/j.pcad.2021.02.006.
10. Sathya VB, Amelia P, Kesava M, et al. Vertebral Artery Stenosis: A Narrative Review.Cureus. 2022,14(8): e28068-e28068; https://doi.org/10.7759/cureus.28068.
11. Tay KY, U-King-Im JM, Trivedi RA, et al. Imaging the vertebral artery. European radiology. 2005,15:1329-1343; https://doi.org/10.1007/s00330-005-2679-z.
12. Montano M, Alman K, Smith MJ, et al. Bow hunter's syndrome: a rare cause of vertebrobasilar insufficiency. Radiology Case Reports. 2021,16(4):867-870; https://doi.org/10.1016/j.radcr.2021.01.041.
13. Zhang LJ. Study on tortuous neck artery and its correlation with vascular lesions of head and neck. Chongqing Medical University. 2021; https://link.oversea.cnki.net/doi/10.27674/d.cnki.gcyku.2021.000145. (in chinese)
14. Zheng XQ, Chen DK, Chen H. Correlation analysis between intracranial aneurysm and internal carotid artery tortuosity. Nerve Injury and Functional Reconstruction. 2021, 16(10): 611-3; https://link.oversea.cnki.net/doi/10.16780/j.cnki.sjssgncj.20201142. (in chinese)
15. Klis KM, Krzyzewskir M, Kwinta BM, et al. Increased tortuosity of basilar artery might be associated with higher risk of aneurysm development. Eur Radiol, 2020,30(10):5625-32; https://doi.org/10.1007/s00330-020-06917-3.
16. Morris, P. D., Narracott, A., von Tengg-Kobligk, H., et al. Computational fluid dynamics modelling in cardiovascular medicine. Heart (British Cardiac Society). 2016,102(1): 18-28; https://doi.org/10.1136/heartjnl-2015-308044.
17. Secomb TW. Hemodynamics. Comprehensive physiology. 2016,6(2):975; https://doi.org/10.1002/cphy.c150038.
18. Cebral JR, Castro MA, Putman CM, et al. Flow-area relationship in internal carotid and vertebral arteries. Physiol Meas. 2008;29(5):585-94; https://doi.org/10.1088/0967-3334/29/5/005.
19. Morris, S. A., Orbach, et al. Increased vertebral artery tortuosity index is associated with adverse outcomes in children and young adults with connective tissue disorders. Circulation. 2011, 124(4): 388-396; https://doi.org/10.1161/CIRCULATIONAHA.110.990549.
20. Zhang Z, Ai X, Xu Y, et al. Impact of craniocervical junction abnormality on vertebral artery hemodynamics: based on computational fluid dynamics analysis. Frontiers in Neurology. 2024, 141244327-1244327; https://doi.org/10.3389/fneur.2023.1244327.
21. Bao J, Gan X, Feng W, et al. Abnormal flow pattern of low wall shear stress and high oscillatory shear index in spontaneous vertebral artery dissection with vertebral artery hypoplasia. Frontiers in Neuroscience. 2023,17:1179963; https://doi.org/10.3389/fnins.2023.1179963.
22. Jiaqiu W, Runxin F, Hao W, et al. Impact of cyclic bending on coronary hemodynamics. Biomechanics and modeling in mechanobiology. 2023,22(2):729-738; https://doi.org/10.1007/s10237-022-01677-z.
23. Kamenskiy AV, Pipinos II, Carson JS, et al. Age and disease-related geometric and structural remodeling of the carotid artery. J Vasc Surg. 2015,62(6):1521-8; https://doi.org/10.1016/j.jvs.2014.10.041.
24. Zhe S, Dengrong J, Peiying L, et al. Age-Related Tortuosity of Carotid and Vertebral Arteries: Quantitative Evaluation With MR Angiography. Frontiers in Neurology. 2022,13858805-858805; https://doi.org/10.3389/fneur.2022.858805.
25. Stemper BD, Yoganandan N, Pintar FA, et al. Anatomical gender differences in cervical vertebrae of size-matched volunteers. Spine (Phila Pa 1976). 2008,33(2): e44-e49; https://doi.org/10.1097/BRS.0b013e318160462a.
26. Ciurica S, Lopez-Sublet M, Loeys BL, et al. Arterial Tortuosity. Hypertension. 2019,73(5):951-60; https://doi.org/10.1161/HYPERTENSIONAHA.118.11647.
27. Satoshi S, Toshihiko N, Hanako Y, et al. A case of severe headache attributed to vertebral artery dissection. JA clinical reports. 2019,5(1):27; https://doi.org/10.1186/s40981-019-0247-9.
28. Gulli G, Khan S, Markus HS. Vertebrobasilar stenosis predicts high early recurrent stroke risk in posterior circulation stroke and TIA. Stroke. 2009,40(8):2732-7; https://doi.org/10.1161/STROKEAHA.109.553859.
29. Jia PL, Xue HC, Li SX, et al. Finite Element Analysis for the Effects of the Descending Aorta Tortuosity on Aortic Hemodynamics. Procedia Computer Science. 2022,209148-156; https://doi.org/10.1016/j.procs.2022.10.109.
30. Qiao A, Dai X, Niu J, et al. Hemodynamics in stented vertebral artery ostial stenosis based on computational fluid dynamics simulations. Computer Methods in Biomechanics and Biomedical Engineering. 2016,19(11):1190-1200. https://doi.org/10.1080/10255842.2015.1123253.
31. Wang DX, Jiang J, Liu H, et al. Geometric modeling and hemodynamic analysis of vertebral artery fenestration based on 3.0T MRA image data. Wisdom and Health. 2021;7(11):1-3+6; https://10.19335/j.cnki.2096-1219.2021.10.001. (in chinese)

32. Sindeev S, Kirschke JS, Prothmann S, et al. Evaluation of flow changes after telescopic stenting of a giant fusiform aneurysm of the vertebrobasilar junction. Biomedical engineering online. 2019,18:1-15; https://doi.org/10.1186/s12938-019-0699-1.
33. Casa LDC, Deaton DH, Ku DN. Role of high shear rate in thrombosis. Journal of vascular surgery. 2015,61(4):1068-1080; https://doi.org/10.1016/j.jvs.2014.12.050.